Reduction of Transients between Steady States in the Continuous Production of High-Impact Polystyrene

Carla V. Luciani, Diana A. Estenoz, and Gregorio R. Meira*

INTEC (Universidad Nacional del Litoral and CONICET), Güemes 3450, Santa Fe (S3000GLN), Argentina

Haydée M. Oliva

Escuela de Ingeniería Química, Universidad del Zulia, Maracaibo, Venezuela

This work theoretically investigates the reduction of transients during changes of grade in a continuous plant for the production of high-impact polystyrene (HIPS). A mathematical model was developed that predicts the global molecular structure and the melt flow index (MFI). The switching times of the off-specs accumulation period were selected on the basis of the admissible MFI ranges. Smoother transitions and reduced off-specs can be produced through a simple readjustment (with respect to the original plant policy) of the two intermediate chain transfer agent (CTA) loads into the batch dissolver. For the transitions that involve a large difference in their MFIs, the off-specs can be reduced by 60%, with respect to the original plant policy, by including a transient feed of CTA into an intermediate stirred reactor.

1. Introduction

The continuous and bulk process for the production of high-impact polystyrene (HIPS), typically involves the following stages: dissolution, prepolymerization, finishing, and devolatilization. In the dissolution stage, a grated polybutadiene (PB) rubber is dissolved in a styrene (St)−solvent mixture. The inhibitor is not eliminated from the monomer stock, to limit the thermal polymerization in the dissolver and feed tank. Also loaded into the batch dissolver are a chain transfer agent (CTA) and a mineral oil. The prepolymerization is well-stirred; it includes a continuous feed of initiator, and it proceeds up to conversions of ∼40%. The finishing stage is gently stirred (to avoid destroying the developed particle morphology), and it requires increasing temperatures to reduce the system viscosity and promote the thermal monomer initiation.

The bulk HIPS process is heterogeneous, because of the thermodynamic incompatibility between the polystyrene (PS) and PB chains. The PS-rich phase is the dispersed phase up to the phase inversion, but thereafter it remains as the continuous phase. The PB chains must be grafted at the beginning of the prepolymerization, to promote the phase inversion and to improve the end-product properties. The mechanical properties of HIPS are determined by its molecular structure and particle morphology.[1−6] The global composition of HIPS is ∼80% of free PS, ∼18% of a St−butadiene graft copolymer, and ∼2% of residual (or unreacted) PB.[7] In the most common "salami" morphology, the rubber particles are ∼2 μm in diameter and contain numerous vitreous occlusions.

Polymerization models are useful for investigating alternative control strategies, and helping to interpret the complex physicochemical phenomena that occur during such processes.[8] In our previous models on the same bulk reaction,[7,9,10] we have assumed homogeneous conditions. This assumption is justified by the fact that the monomer and the initiator are almost evenly distributed between the (PS-rich and PB-rich) phases.[11] In Estenoz et al.,[7] we have previously modeled the investigated plant. The developed model predicted the global molecular structure, and it was adjusted to the steady state (SS) measurements of two HIPS grades.[7]

In relation with continuous PS processes, relatively few publications have appeared that optimize the transitions between SSs. Na and Rhee[12] developed a dynamical model for simulating a continuous St homopolymerization and developed a nonlinear control strategy for optimizing the changes of grade. For a HIPS process that has been performed in a single continuous stirred tank reactor (CSTR), Flores et al.[13] optimized the transitions between unstable SSs, through manipulation of the cooling water and the initiator feed. For a series of seven CSTRs, Flores et al.[14] performed a (SS and nonlinear) bifurcation analysis that is potentially useful for the process design, operation, and control.

This article intended to reduce the off-specs that are generated during changes of grade in a continuous HIPS plant. To this effect, the mathematical model by Estenoz et al.[7] was extended to estimate the melt flow index (MFI) of the final product. The new model was validated with SS and transient measurements of the three most important HIPS grades.

2. Experimental Work

Industrial Process. Figure 1 schematically represents the investigated process (Estizulia C. A., Maracaibo, Venezuela). The batch dissolver (R_1) operates in an 8-h cycle. At the end of each batch, the dissolver content is discharged into the feed tank (R_2) within ∼20 min. The feed tank presents a continuous output flow and a discontinuous input; therefore, it exhibits a periodic-level oscillation. The continuous process includes two CSTRs (R_3 and R_4), two vertical reactors (R_5 and R_6), a preheater (R_7), and a devolatilizer. Except for the chemical initiator that is continuously injected

* To whom correspondence should be addressed. Tel.: 0054-342-455-9174. Fax: 54-342-455-0944. E-mail: gmeira@ceride.gov.ar.

10.1021/ie050657z CCC: $30.25 © 2005 American Chemical Society
Published on Web 09/28/2005

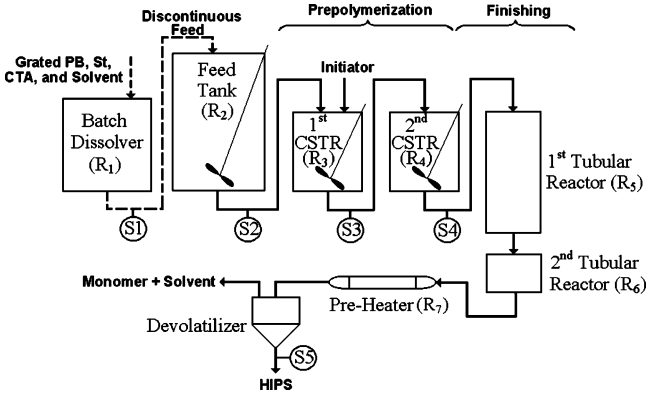

Figure 1. Diagram of the continuous industrial process. Features S1−S5 indicate the sampling points for the steady state (SS) and transient measurements. (Courtesy of Estizulia C. A., Maracaibo, Venezuela.)

Table 1. Principal Characteristics of the Three Most Important High-Impact Polystyrene (HIPS) Grades[a]

property	grade A (PS 4600)	grade B (PS 4000)	grade C (PS 4320)
impact strength [lb-ft/in]	2.2	2.0	1.7
elongation at break [%]	50	58	50
yield strength [lb-ft/in^2]	3600	3700	2800
residual St [wt %]	0.1	0.1	0.1
volatile content [wt %]	0.2	0.2	0.2
mineral oil content [wt %]	2.7	2.0	3.1
$\bar{M}_w$ of the free PS [g/mol]	200 000	180 000	140 000
MFI range [g/10 min]	2.6−3.6	3.0−4.0	6.0−9.0

[a] The commercial name for each grade is given in parentheses.

into R_3, all the other reagents are fed into R_1. The prepolymerization occurs in R_3 and R_4, whereas the finishing occurs in R_5 and R_6. In the devolatilizer, the solvent and unreacted monomer are stripped from the polymer and mineral oil.

Table 1 presents the quality specifications of the three most important HIPS grades. Grade A is a relatively hard material that is used for producing thick thermoformable plates. It exhibits high PS molecular weights and a low MFI (or a high melt viscosity). Grade B is used for producing thinner plates, and grade C is used for manufacturing injection-molded articles. The MFI ranges of grades A and B are overlapping (the lower molecular weights of grade B are compensated by its also-lower mineral oil content).

Table 2 presents the SS recipes and reaction conditions. In R_1 and R_2, the temperatures are high enough to promote some thermal monomer initiation. In the preheater, the temperature is the highest. In the devolatilizer, the polymerization is negligible, because the monomer is almost completely stripped from the melt polymer. Thus, the polymerizations occur in "reactors" R_1−R_7. The quality of the devolatilizer polymer outlet coincides with the quality of the final product.

Measurements. Samples were taken at points S1−S5 of Figure 1, and the following analyses were performed at our laboratories. The total polymer mass (m_P) was determined, after isolating the polymer from the monomer, solvent, and mineral oil, as follows: (i) 10 g of sample (m_S) were dissolved into 35 mL of toluene that contained hydroquinone as an inhibitor; and (ii) the total polymer was precipitated in methanol, filtered, and dried under vacuum at 30 °C until constant weight. The free PS mass (m_{PS}) then was isolated from the insoluble (i.e., graft copolymer + unreacted PB), through the following solvent extraction procedure: (a) 0.3 g of dry (oil-free) polymer was introduced into a 10-mL vial containing a 50:50 solution of methyl ethyl ketone (MEK) and dimethyl formamide (DMF); (b) the mixture was agitated for 12 h and then centrifuged for 2 h at 12 000 rpm and 10 °C; (c) the soluble fraction was separated, while the insoluble was redispersed into another 10 mL of MEK/DMF; (d) the procedure was repeated twice, and the three PS solutions were mixed together; and (e) the free PS was precipitated in methanol, filtered, and dried under vacuum until constant weight. The mass aliquots (with respect to m_S) of the initial mineral oil, PB, and St (m°_{Oil}, m°_{PB}, and m°_{St}, respectively) were directly estimated from the recipe.

The following global variables were calculated in several reactors. The solid content is the ratio between the mass of nonvolatiles (i.e., polymers + mineral oil) and the total sample mass, and it was obtained from the relation $S_C = (m_P + m^\circ_{Oil})/m_S$. The polymer content is the ratio between the oil-free polymer mass and the total sample mass; and it was obtained from the relation $P_C = m_P/m_S$. The monomer conversion is the ratio between the outlet mass flow rate of the (free and

Table 2. Steady State (SS) Recipes and Reaction Conditions for a Constant Feed Rate of 1.8 L/s into R_3

	grade A	grade B	grade C
	(a) Recipe into R_1		
styrene (St)	44074 kg	44777 kg	45288 kg
polybutadiene (PB)[a]	3667 kg	3120 kg	3240 kg
tert-dodecyl mercaptane (CTA)	6.0 kg	9.0 kg	20.2 kg
ethylbenzene (solvent)	6667 kg	6667 kg	5556 kg
4-*tert*-butyl catechol (inhibitor)	0.7 kg	0.8 kg	0.8 kg
mineral oil[b]	1012 kg	929 kg	1223 kg
	(b) Recipe into R_3		
tert-butyl peroctoate (initiator)[c]	0.00082 mol/s	0.0014 mol/s	0.0018 mol/s
	(c) Reaction Volumes and Temperatures		
R_1 (64.5 m^3)	70 °C	70 °C	70 °C
R_2 (52.5 m^3)	75 °C	75 °C	75 °C
R_3 (18.6 m^3)	125 °C	123 °C	119 °C
R_4 (18.6 m^3)	126 °C	124 °C	122 °C
R_5 (19.2 m^3)	142 °C	142 °C	142 °C
R_6 (6.6 m^3)	155 °C	154 °C	155 °C
R_7 (0.5 m^3)	242 °C	242 °C	242 °C

[a] Average molecular weights of the initial PB: $\bar{M}_{n,PB}$ = 102 000 g/mol, and $\bar{M}_{w,PB}$ = 218 000 g/mol. [b] Mineral oil densities at 25 and 50 °C are 934.3 and 853.1 kg/m^3, respectively. Zero-shear viscosities of the mineral oil at 25, 57, and 82 °C are 0.140, 0.026, and 0.013 Pa s, respectively. [c] Initiator concentration at R_3 inlet: [I] = 801 mol/m^3.

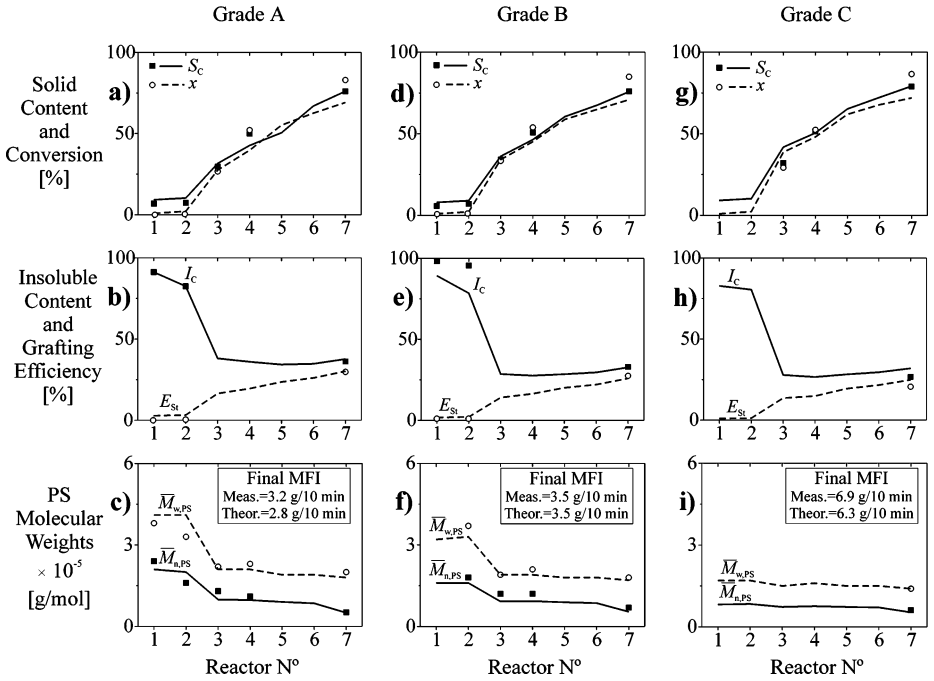

Figure 2. SS measurements (in symbols) and model predictions (in lines) for the three investigated HIPS grades. The top row of graphs (a, d, and g) depict the solid content and conversion, the middle row of graphs (b, e, and h) depict the insoluble content and grafting efficiency, and the bottom row of graphs (c, f, and i) depict the free PS molecular weights. The R_1 values correspond to the end of the batch operation.

grafted) PS chains and the inlet mass flow rate of St (see eq A.33 in Appendix A). However, the monomer conversion was experimentally determined through the relation $x = (m_P - m^\circ_{PB})/m^\circ_{St}$. The insoluble content is the ratio between the mass of PB + graft copolymer and the total polymer mass; and it was obtained from the relation $I_C = (m_P - m_{PS})/m_P$. The grafting efficiency (E_{St}) is the ratio between the mass of grafted PS and the total mass of polymerized St, and it was obtained from the relation $E_{St} = (m_P - m^\circ_{PB} - m_{PS})/(m_P - m^\circ_{PB})$. For calculating S_C, x, and E_{St}, either m°_{Oil}, m°_{PB}, or m°_{St} were required. For this reason, S_C, x, and E_{St} could be only determined in the SSs, but not during the transients. In contrast, P_C and I_C were determined both in the SSs and during the transients.

Size exclusion chromatography (SEC) was applied to measure the molecular weight distribution (MWD) of the initial PB, and the MWDs of the free PS in reactors R_1–R_4 and R_7. A Waters-Breeze chromatograph that was fitted with a complete set of μ-Styragel columns (Waters Ass.) was used. Even though the MWD of the initial PB is not presented here, for space reasons, its averages are given in Table 2.

The MFI of the final product was determined at the plant laboratories, following ASTM D1238. The extrusion plastometer was operated at 200 °C, and it was weighted with a 5-kg load. The MFI is mainly dependent on the $\overline{M}_w$ of the continuous PS phase and on the mineral oil content. For the mineral oil, its viscosity and density are presented in Table 2.

Steady States. The SS recipes are given in Table 2. Their main differences are (i) the feed flows of initiator into R_3 and (ii) the loads of CTA and mineral oil into R_1.

Figure 2 presents the SS measurements of the final MFI and of the solid content, insoluble content, and free PS molecular weights in reactors R_1–R_4 and R_7. The monomer conversion was obtained from the solid content, and the grafting efficiency was obtained from the insoluble content (see Figure 2). The insoluble content and grafting efficiencies in R_3 and R_4 were discarded and are not presented in panels b, e, and h in Figure 2. The reason was that they exhibited large errors in excess, because of an abnormal accumulation of a precipitate in R_3 and R_4. Fortunately, however, the PS molecular weights were unaffected by the said precipitate and are shown in panels c, f, and i in Figure 2.

The following can be noted:

(a) The polymer content and monomer conversion both increase along the train.

(b) The insoluble content is high in the first two "reactors", because of their relatively large amount of PB.

(c) The grafting efficiency is negligible in R_1 and R_2, it increases in R_3 (because of the initiator feed), and it is highest in R_7 (because of its very high temperature).

(d) The PS molecular weights are high in R_1 and R_2, because of the absence of the chemical initiator and the high probability of termination by recombination, with respect to termination by chain transfer to the monomer.

(e) The PS molecular weights decrease dramatically in the last reactors, because of the highly increased rate of the chain transfer to the monomer reaction.

Changes of Grade. In the investigated process, large amounts of off-specs were produced. This is because a high frequency of the changes of grade (2–3 per week) is combined with a large mean residence time of the reactor train (of ~30 h). In the following discussion, consider the direct and inverse transitions between grades A and B, and those between grades A and C. In all four transitions, the total feed flow was fixed at 1.8 L/s.

Table 3 presents the plant policies for the changes of grade. Between the initial and final recipes into the dissolver R_1, two intermediate batches were applied that were intended to accelerate the transitions into the final grade. The initial time of a change of grade was adopted

Table 3. Plant Policies for the Transitions A⇆B and A⇆C at a Fixed Feed Rate into R_3 of 1.8 L/s

	Batch Loads into Dissolver R_1 (kg)			
change of grade[a]	initial grade[b]	1st intermittent batch[c]	2nd intermittent batch[d]	final grade[e]
(a) A → B				
styrene, St	44074	45557	43933	44777
polybutadiene, PB	3667	2956	3135	3120
tert-dodecyl mercaptane, CTA	6.0	13.0	9.8	9.0
ethylbenzene (solvent)	6667	6667	6667	6667
4-*tert*-butyl catechol (inhibitor)	0.7	0.8	0.8	0.8
mineral oil	1012	690	770	929
(b) B → A				
styrene, St	44777	43700	44090	44074
polybutadiene, PB	3120	3954	2653	3667
tert-dodecyl mercaptane, CTA	9.0	1.9	5.2	6.0
ethylbenzene (solvent)	6667	6667	6667	6667
4-*tert*-butyl catechol (inhibitor)	0.8	0.7	0.7	0.7
mineral oil	929	1195	10990	1012
(c) A → C				
styrene, St	44074	45612	45055	45288
polybutadiene, PB	3667	3313	3441	3240
tert-dodecyl mercaptane, CTA	6.0	37.3	25.4	20.2
ethylbenzene (solvent)	6667	4973	5586	5556
4-*tert*-butyl catechol (inhibitor)	0.7	0.8	0.8	0.8
mineral oil	1012	1334	1218	1223
(d) C → A				
styrene, St	45288	43545	44103	44074
polybutadiene, PB	3240	3788	3660	3667
tert-dodecyl mercaptane, CTA	20.2	0.0	5.1	6.0
ethylbenzene (solvent)	5556	7249	6636	6667
4-*tert*-butyl catechol (inhibitor)	0.8	0.7	0.7	0.7
mineral oil	1223	902	1018	1012

[a] In R_3, linear ramps of the initiator feed and the temperature are imposed during 3.5 h, starting 2 h after t_0 (the time when the first intermittent batch ends its discharge into the feed tank). In R_4, a linear temperature ramp is imposed during 6 h, starting 3 h after t_0. [b] Applied at $t = t_0 - 8$ h. [c] Applied at $t_0 = 0$ h. [d] Applied at $t = t_0 + 8$ h. [e] Applied at $t = t_0 + 16$ h.

as the moment when the first intermediate dissolver batch is loaded into the feed tank R_2. For the changes of grade that involve a reduction of the molecular weights, the intermediate CTA are larger than any of the SS values. For the changes of grade that involve increasing the molecular weights, the intermediate CTA loads are smaller than any of the SS values. During the changes of grade, linear ramps were applied to the initiator feed flow into R_3, and to the temperatures of R_3 and R_4 (see Table 3). For the given total feed flow, the plant product continued to be accumulated as the initial grade between $t = 0$ and $t_1 = 5.5$ h (the first switching time). The intermediate off-specs then were accumulated between $t_1 = 5.5$ h and $t_2 = 14$ h. At t_2, the MFI of the final product was analyzed to verify if it was within the specifications of the final grade; if so, then the plant product began to be accumulated as the final grade (the second switching time).

The transient measurements are represented in panels a, d, g, and j in Figures 3 and 4. For the transition A→B, Figure 3 presents the measurements (in R_2, R_3, R_4, and R_7) of P_C, I_C, and the PS molecular weights, whereas Figure 4a presents the MFI measurements of the final product. The I_C measurements in R_3 and R_4 were discarded, because of their large errors in excess. For the transitions B→A and A⇆C, only the MFI measurements are presented (Figure 4d, 4g, and 4j). Also shown in Figure 4a, 4d, 4g, and 4j are the admissible bands of the MFI specifications (see Table 1).

The MFIs of Figure 4g and 4j show overshoots and undershoots. For the grades A and B, their admissible MFI bands are overlapping. In contrast, the MFI bands of grades A and C are well-separated. In the investigated transitions, the MFI measurements at $t_2 = 14$ h were all within specifications of the final grade. For that reason, the off-specs accumulation periods of all four transitions were coincident and are given by $t_1 = 5.5$ h and $t_2 = 14$ h. Because the MFI specifications of grades A and B are overlapping, then the MFI measurements of the transitions A⇆B were within specifications at all times. Thus, through a simple modification of the switching policy, it would be possible to implement the A⇆B transitions without the generation of off-specs.

3. Mathematical Modeling

The polymerization model is almost identical to that of Estenoz et al.[7] It is based on the kinetic mechanism of Table 4. Following Estenoz et al.,[7] the process was assumed to be homogeneous, and each of the tubular reactors (R_5 and R_6) were modeled as a series of five continuously stirred tank reactors (CSTRs). Previous simulation results have shown a negligible final concentration of H-shaped cross-linked copolymer.[7] For this reason, the mechanism of Table 4 does not include the recombination of free radicals to produce a cross-linked copolymer.

The global mass balance was derived from the global kinetics of Table 4, and it is represented by eqs A.1−A.8, A.15, and A.21−A.24 in Appendix A. They predict the conversion, solid content, polymer content, grafting efficiency, insoluble content, oil volume fraction, rubber volume fraction, and free PS average molecular weights ($\overline{M}_{n,PS}$ and $\overline{M}_{w,PS}$). The detailed mass balance was derived from the detailed kinetics of Table 4, and it is represented by eqs A.16−A.17 in Appendix A. These equations predict the average molecular weights of the residual PB ($\overline{M}_{n,PB}$, $\overline{M}_{w,PB}$), the average molecular weights of the graft copolymer ($\overline{M}_{n,C}$ and $\overline{M}_{w,C}$), and the average number of PS branches per copolymer molecule ($\bar{r}_n$).

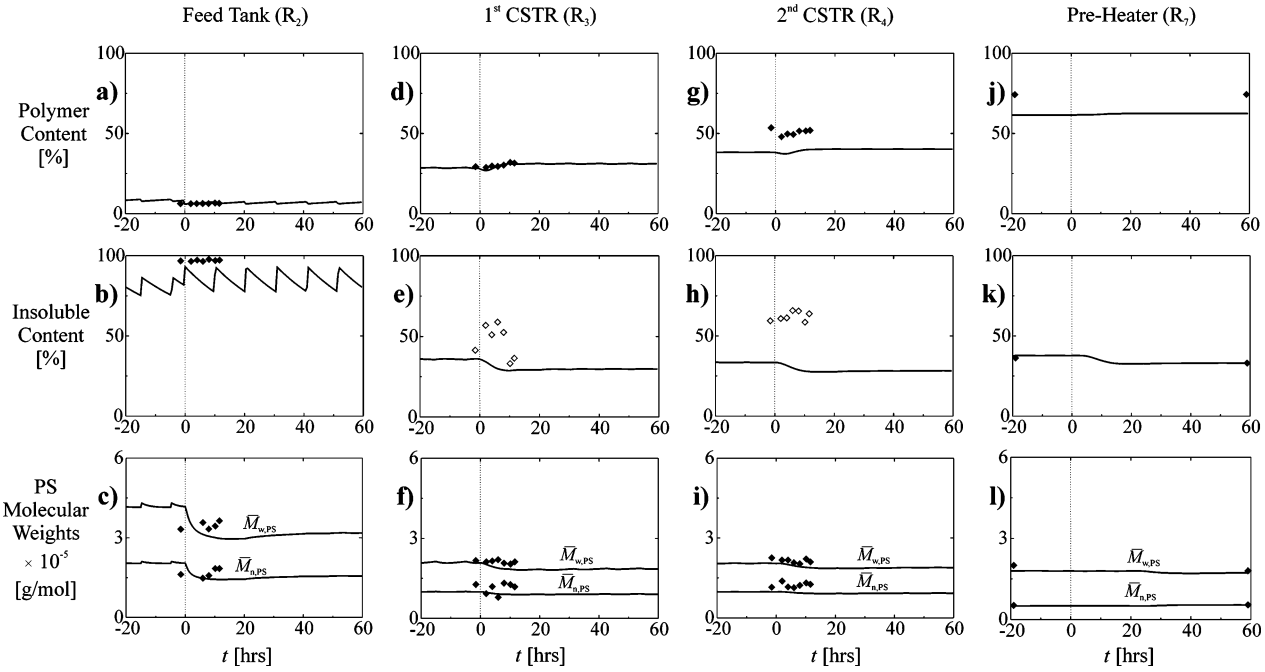

Figure 3. Plant policy for the A→B transition in reactors R_2, R_3, R_4, and R_7. The top row of graphs (a, d, g, and j) depicts the evolution of the polymer content, the middle row of graphs (b, e, h, and k) depicts the evolution of the insoluble content, and the bottom row of graphs (c, f, i, and l) depicts the evolution of the free PS molecular weights. Legend throughout figure is as follows: (◆) valid measurements, (◇) discarded measurements, and (—) simulated results.

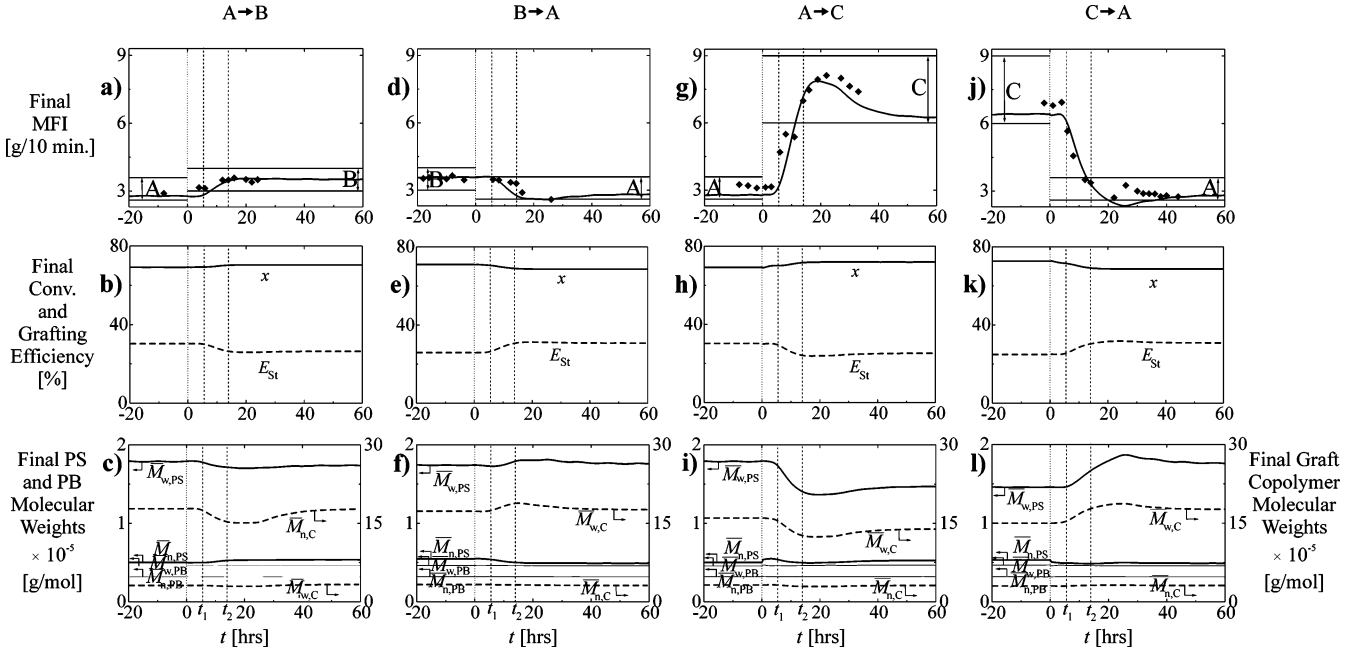

Figure 4. Plant policy for the A⇆B and A⇆C transitions. The top row of graphs (a, d, g, and j) depict the evolution of the final MFI and MFI specification bands, the middle row of graphs (b, e, h, and k) depicts the evolution of the final conversion and grafting efficiency, and the bottom row of graphs (c, f, i, and l) depicts the evolution of the final average molecular weights of the three HIPS components (free PS, residual PB, and graft copolymer). Legend throughout figure is as follows: (◆) experimental measurements and (—) simulated results. Switching times are $t_1 = 5.5$ h and $t_2 = 14$ h.

The polymerization model of Appendix A was combined in series with the MFI model of Appendix B. Appendix B is based on the model by Seavey et al.,[15] combined with an independent estimation of the apparent viscosity function $\eta(\dot{\gamma})$. The MFI model inputs are the plastometer characteristics (dimensions and operating conditions) and the final HIPS characteristics. The final HIPS characteristics are determined by the polymerization model and consist of the volume fractions of the four HIPS components (free PS, graft copolymer, residual PB, and mineral oil), and the weight-average molecular weight of the free PS ($\overline{M}_{w,PS}$). The exponential relationship between $\overline{M}_{w,PS}$ and the melt viscosity of eq B.5 determines that small variations in $\overline{M}_{w,PS}$ are considerably amplified in the MFI.

The model parameters are given in Table 5. Most of the parameters were directly taken from the literature.[7]

Table 4. Kinetic Mechanism

global kinetics $s, n, m = 1, 2, 3, \ldots$	detailed kinetics $b, b_1, n, m = 1, 2, 3, \ldots; s, s_1, s_2, g, r = 0, 1, 2, \ldots$
Initiation	
$I \xrightarrow{k_d} 2I^\bullet$	$I \xrightarrow{k_d} 2I^\bullet$
$I^\bullet \xrightarrow{k_{i1}} S_1^\bullet$	$I^\bullet \xrightarrow{k_{i1}} S_1^\bullet$
$I^\bullet + P \xrightarrow{k_{i2}} P_0^\bullet$	$I^\bullet + P_g(s,b) \xrightarrow{k_{i2}} P_{0,g}^\bullet(s,b)$
Thermal Initiation	
$3St \xrightarrow{k_{i0}} 2S_1^\bullet$	$3St \xrightarrow{k_{i0}} 2S_1^\bullet$
Propagation	
$S_{s-1}^\bullet + St \xrightarrow{k_p} S_s^\bullet$	$S_{s-1}^\bullet + St \xrightarrow{k_p} S_s^\bullet$
$P_0^\bullet + St \xrightarrow{k_{p0}} P_1^\bullet$	$P_{0,g-1}^\bullet(s,b) + St \xrightarrow{k_{p0}} P_{1,g}^\bullet(s,b)$
$P_{n-1}^\bullet + St \xrightarrow{k_p} P_n^\bullet$	$P_{n-1,g}^\bullet(s,b) + St \xrightarrow{k_p} P_{n,g}^\bullet(s,b)$
Chain Transfer to the Monomer	
$S_s^\bullet + St \xrightarrow{k_{fm}} P_S(s) + S_1^\bullet$	$S_s^\bullet + St \xrightarrow{k_{fm}} P_S(s) + S_1^\bullet$
$P_n^\bullet + St \xrightarrow{k_{fm}} P + S_1^\bullet$	$P_{n,g}^\bullet(s-n,b) + St \xrightarrow{k_{fm}} P_g(s,b) + S_1^\bullet$
$P_0^\bullet + St \xrightarrow{k'_{fm}} P + S_1^\bullet$	$P_{0,g}^\bullet(s,b) + St \xrightarrow{k'_{fm}} P_g(s,b) + S_1^\bullet$
Chain Transfer to the PB or the Copolymer	
$S_n^\bullet + P \xrightarrow{k_{fg}} P_S(n) + P_0^\bullet$	$S_n^\bullet + P_g(s,b) \xrightarrow{k_{fg}} P_S(n) + P_{0,g}^\bullet(s,b)$
$P_n^\bullet + P \xrightarrow{k_{fg}} P + P_0^\bullet$	$P_{n,g-1}^\bullet(s-n,b) + P_r(s_1,b_1) \xrightarrow{k_{fg}} P_g(s,b) + P_{0,r}^\bullet(s_1,b_1)$
Chain Transfer to the CTA	
$S_s^\bullet + X \xrightarrow{k_{fx}} P_S(s) + S_1^\bullet$	$S_s^\bullet + X \xrightarrow{k_{fx}} P_S(s) + S_1^\bullet$
$P_n^\bullet + X \xrightarrow{k_{fx}} P + S_1^\bullet$	$P_{n,g-1}^\bullet(s-n,b) + X \xrightarrow{k_{fx}} P_g(s,b) + S_1^\bullet$
$P_0^\bullet + X \xrightarrow{k'_{fx}} P + S_1^\bullet$	$P_{0,g}^\bullet(s,b) + X \xrightarrow{k'_{fx}} P_g(s,b) + S_1^\bullet$
Chain Transfer to the Inhibitor	
$S_s^\bullet + Z \xrightarrow{k_{fz}} P_S(s) + Z^\bullet$	$S_s^\bullet + Z \xrightarrow{k_{fz}} P_S(s) + Z^\bullet$
$P_n^\bullet + Z \xrightarrow{k_{fz}} P + Z^\bullet$	$P_{n,g-1}^\bullet(s-n,b) + Z \xrightarrow{k_{fz}} P_g(s,b) + Z^\bullet$
$P_0^\bullet + Z \xrightarrow{k'_{fz}} P + Z^\bullet$	$P_{0,g}^\bullet(s,b) + Z \xrightarrow{k_{fz}} P_g(s,b) + Z^\bullet$
Termination by Recombination	
$S_{s-n}^\bullet + S_n^\bullet \xrightarrow{k_{tc}} P_S(s)$	$S_{s-n}^\bullet + S_n^\bullet \xrightarrow{k_{tc}} P_S(s)$
$P_m^\bullet + S_n^\bullet \xrightarrow{k_{tc}} P$	$P_{m,g-1}^\bullet(s-m-n,b) + S_n^\bullet \xrightarrow{k_{tc}} P_g(s,b)$
$P_0^\bullet + S_n^\bullet \xrightarrow{k''_{tc}} P$	$P_{0,g-1}^\bullet(s-n,b) + S_n^\bullet \xrightarrow{k''_{tc}} P_g(s,b)$

However, four of the parameters were adjusted to fit the measurements of Figure 2, which correspond to the SSs of the three investigated grades. Figure 2 also presents the measured and predicted values of the final MFIs. Also, note that, in Figure 2, only the abscissas at integer reactor numbers have a physical meaning. As in Estenoz et al.,[7] three of the kinetic constants were adjusted (within published ranges). To this effect, the following sequential procedure was applied: (i) adjust the rate constant of thermal monomer initiation k_{i0}, to reproduce the solid content; (ii) adjust the rate constant of transfer to the rubber k_{fg}, to reproduce the insoluble content; and (iii) adjust the rate constant transfer of transfer to the CTA k_{fx}, to reproduce the PS molecular weights. In each of these steps, a Nelder–Mead algorithm[21] was used to minimize the absolute value of the difference between the measurements and the model predictions. To fit the final MFI measurements, the constant A of eq B.4 in Appendix B was adjusted. A quite reasonable agreement between the measurements and the theoretical predictions is observed (Figure 2).

After its adjustment, the model was validated with the transient measurements of Figures 3, 4a, 4d, 4g, and 4j. A reasonable agreement is again observed. In R_2, some of the predicted variables exhibit periodic oscillations (Figure 3b and 3c). Such oscillations are caused by the oscillations in the level R_2 and are almost completely smeared off in R_3.

Some additional model predictions are presented in Figures 5, 4b, 4c, 4e, 4f, 4h, 4i, 4k, and 4l. Figure 5 presents the SS predictions of the residual PB molecular weights, graft copolymer molecular weights, and average number of PS branches per copolymer molecule. The PB molecular weights fall along the train, because longer PB chains exhibit a higher probability of grafting than shorter chains. For that same reason, the graft copolymer molecular weights initially decrease, but then increase, because of the grafting–overgrafting process. The final drop of $\overline{M}_{n,C}$ in R_7 is a consequence of a late grafting of the (shortest and mainly unbranched) PB chains. Although not shown, the molecular weights of the grafted PS branches decrease in R_3 (because of the initiator addition), and then further decrease in the last reactors (because of their very high temperatures). In R_7, there is a large increase in the number of grafted branches per molecule. This is a consequence of the large effect of temperature on the activation energy of the transfer to the rubber rate constant. According to the model, the final copolymer exhibits in average of ~10 PS branches per molecule.

Panels b, c, e, f, h, i, k, and l in Figure 4 present the predicted transient evolutions of the final conversion,

Table 5. Model Parameters

	value	reference
	(a) Kinetic Constants	
f	0.57	7
k_d	$9.1 \times 10^{13}\ e^{-14850/T}$	7
k_{tc} and k''_{tc}		7
expression	$1.7 \times 10^6\ e^{-(839/T)-2(C_1\phi_P+C_2\phi_P^2+C_3\phi_P^3)}$	
C_1	$2.57 - 0.00505T$	
C_2	$9.56 - 0.0176T$	
C_3	$-3.03 + 0.00785T$	
k_p, k_{p0}, and k_{i1}	$1.0 \times 10^4\ e^{-3557/T}$	7
k_{fx}, k'_{fx}	$7000\ e^{-3020/T}$	adjusted in this work
k_{fz}, k'_{fz}	$5.9 \times 10^{13}\ e^{-11052/T}$	7
k_{i0}	$0.11\ e^{-14092/T}$	adjusted in this work
k_{fm}, k'_{fm}	$6.6 \times 10^4\ e^{-7247/T}$	7
k_{i2}	$2000\ e^{-3557/T}$	7
k_{fg}	$3.0 \times 10^6\ e^{-8556/T}$	adjusted in this work
	(b) MFI Model	
A[a]	1.3	adjusted in this work
B[a]	0.68	16
n'[b]	0.75	17
	(c) Physical Constants	
ρ_{St}	$923.7 - 0.918(T - 273)$	18
ρ_{Sv}	$896.0 - 1.200(T - 273)$	18
ρ_{PS}	$1084.8 - 0.605(T - 273)$	19
ρ_{PB}	$\{1.097 \times 10^{-3} + 7.679 \times 10^{-7}(T - 273) - 2.222 \times 10^{-10}(T - 273)^2\}^{-1}$	20
ρ_{Oil}	$1001.6 - 2.692(T - 273)$	adjusted in this work[c]
η_{Oil}	$e^{-17.0+(4460.7/T)}$	adjusted in this work[c]

[a] See eq B.4. [b] See eq B.1. [c] From measurements of Table 2.

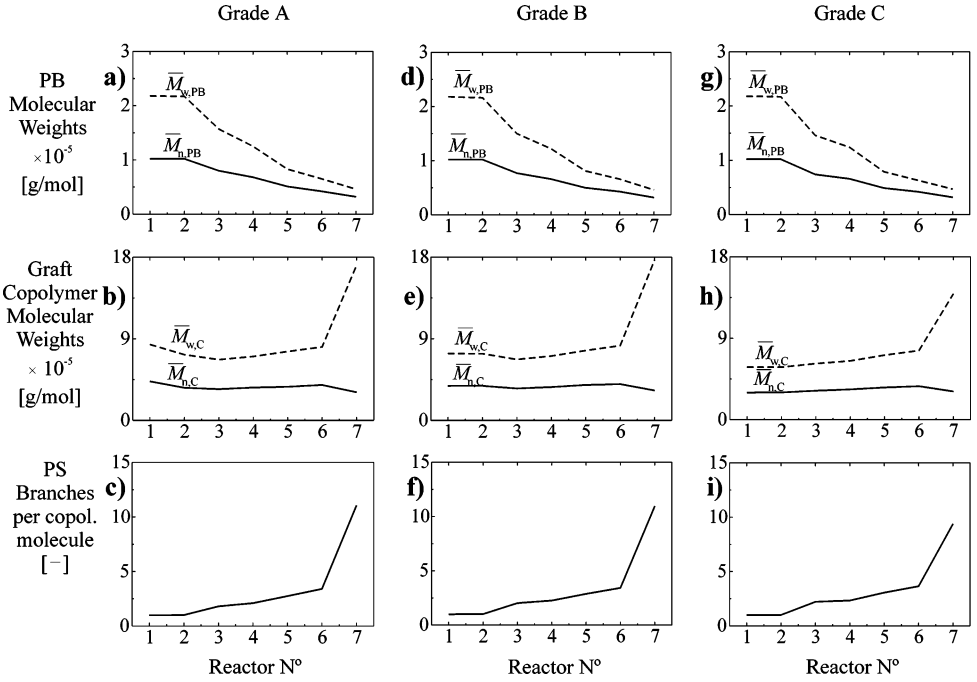

Figure 5. SS model predictions for the three investigated HIPS grades. The top row of graphs (a, d, and g) depicts the residual PB molecular weights, the middle row of graphs (b, e, and h) depicts the graft copolymer molecular weights, and the bottom row of graphs (c, f and i) depicts the PS branches per copolymer molecule.

grafting efficiency, and average molecular weights. Note the following:

(i) Because of the system nonlinearity, the direct and inverse transitions are asymmetric.

(ii) The conversion and grafting efficiency transitions are smooth, because their SS values are all quite similar (Figure 4b, 4e, 4h, and 4k).

(iii) For the same previous reason, the molecular weights of the residual PB and the graft copolymer are affected only slightly by the changes of grade.

4. Improved Changes of Grade (Simulated Results)

As we have seen, a simple modification of the switching policy would produce A⇆B transitions without generation of off-specs. For this reason, consider in what follows only improving the changes of grade A⇆C. To this effect, dynamic optimizations were conducted that involved minimizing the off-specs accumulation period ($t_2 - t_1$). Also, the optimizations were numerically per-

Table 6. Changes of Grade A⇆C: Global Off-specs According to the Three Investigated Policies

	A → C	C → A
Normal Plant Policy		
off-spec accumulation period, t_2-t_1 [h]	8.50	8.50
off-spec volume [m^3]	30.09	30.99
(1) Readjusted Plant Policy		
off-spec accumulation period, t_2-t_1 [h]	5.76	6.39
off-spec volume [m^3]	21.28	23.21
(2) Readjusted Policy + Transient Feed of CTA		
off-spec accumulation period, t_2-t_1 [h]	3.46	4.10
off-spec volume [m^3]	12.51	14.02

formed by application of a Nelder−Mead Simplex algorithm. The switching times were determined as follows: t_1 corresponds to the time when the final product abandons the admissible MFI range of the initial grade, and t_2 corresponds to the time when the final product enters (and remains) within the admissible MFI range of the final grade. The SS conversions of grades A and C are both quite similar (Figure 2a and 2g). For this reason, the minimization of t_2-t_1 simultaneously almost minimizes the off-spec polymer mass and the off-spec polymer volume.

First Level of Improvement: Readjustment of the Intermediate Loads of CTA into the Dissolver R_1. Consider a simple readjustment of the two intermediate loads of CTA into the dissolver R_1, while maintaining all the other inputs as in their normal plant policy values of Table 3. The off-specs accumulation periods were minimized through an iterative readjustment of the two intermediate CTA loads into R_1. The algorithm was initialized with the original plant policies.

The global off-spec results are presented in Table 6 (where also the off-specs of the normal plant operation are presented for comparison). The resulting transient evolutions are given in Figure 6. The readjusted loads are similar to those of the original plant policy, but generally are less abrupt (see Figure 6a and 6d). In the plant policy, the two intermediate CTA loads are either larger or smaller than the initial and final SS values. In the readjusted policies, the directions of change of the first intermediate loads coincide with the plant policies; but this is not the case of the second intermediate loads. The new second intermediate loads seem to compensate for the (moderate) overreactions that would be otherwise introduced by the first intermediate loads.

The final MFIs show fast transitions with negligible overshoots or undershoots (see Figure 6c and 6f). For the transitions A→C and C→A, the accumulation periods resulted ($t_1 = 7.3$ h, $t_2 = 13.1$ h) and ($t_1 = 6.2$ h, $t_2 = 12.6$ h), respectively. With these new periods, the intermediate off-specs are reduced by ∼30%, with respect to the original plant policy (Table 6).

Second Level of Improvement: an Intermediate Transient Feed of CTA is Admitted. Consider reducing the accumulation periods of A⇆C, with respect to the results of Figure 6. To this effect, a transient feed of CTA is now admitted into R_4. This plant modification is technically feasible, because the rapid diffusion of the new added CTA into the reaction mixture is ensured by the reactor stirring and by the relatively low viscosity in R_4. Consider subdividing the plant into two subsystems in series. The first subsystem (R_1-R_3) is controlled by manipulating the two intermediate loads into R_1. The second subsystem (R_4-R_7) is simultaneously controlled by manipulating a transient feed of CTA into R_4. The transition A→C involves reducing the molecular weights, whereas C→A involves increasing the molecular weights. The former transition is simpler to perform than the latter, because a CTA feed can always be added but not extracted.

The CTA feed profiles into R_4 were specified through "staircase" functions of four equally spaced steps. The functions were defined by the total addition time and by the (constant) feed flows during each of the four

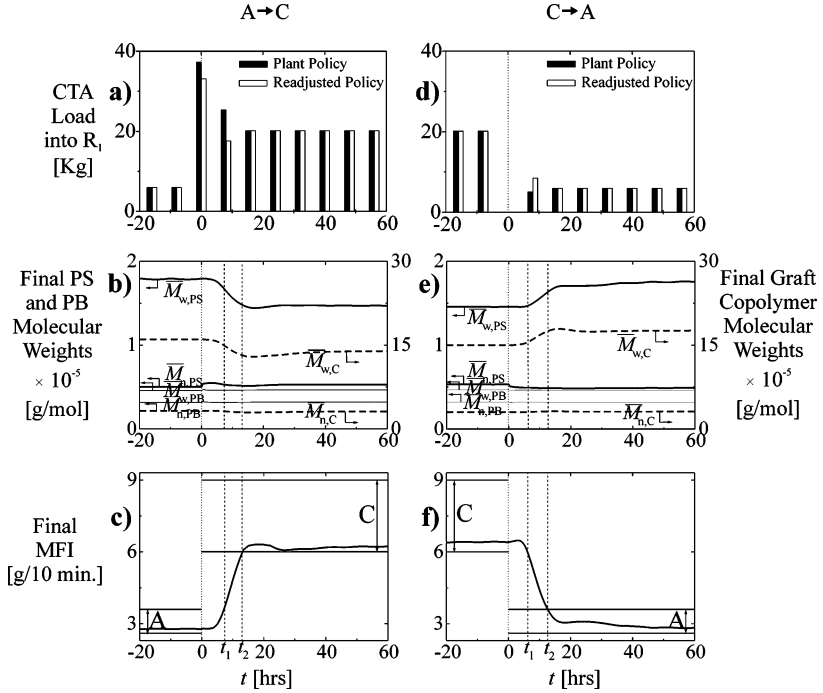

Figure 6. Readjusted plant policy of the intermediate loads of chain transfer agent (CTA) into R_1, for the transitions A⇆C: (a and d) applied loads of CTA into R_1, according to the original and readjusted plant policies; (b and e) evolution of the final average molecular weights of the three HIPS components (free PS, residual PB, and graft copolymer); and (c and f) evolution of the final MFI. Switching times of the A→C transition were $t_1 = 7.3$ h and $t_2 = 13.1$ h. Switching times of the C→A transition were $t_1 = 6.2$ h and $t_2 = 12.6$ h.

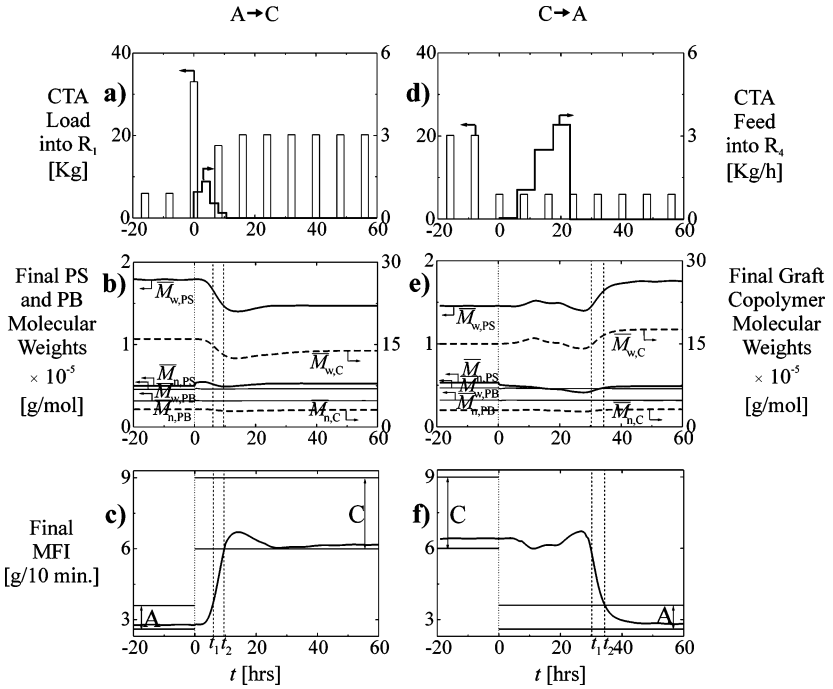

Figure 7. Second level of improvement of the plant policy, admitting a transient feed flow of CTA into R_4. For the A→C transition, the policy requires accelerating the change as much as possible, whereas, for the C→A transition, the policy requires delaying the change as much as possible: (a and d) evolution of manipulated variables (i.e., CTA loads into R_1 and transient CTA feed profile into R_4); (b and e) evolution of the final average molecular weights of the three HIPS components (free PS, residual PB, and graft copolymer); and (c and f) evolution of the final MFI. Switching times for the transition A→C were $t_1 = 6.0$ h and $t_2 = 9.5$ h. Switching times for the transition C→A were $t_1 = 30.2$ h and $t_2 = 34.3$ h.

steps. The off-specs accumulation periods were minimized through an iterative readjustment of the five parameters that define the CTA profile.

For the change of grade A→C, we aimed at producing a fast and early transition. To this effect, we adopted the readjusted plant policy of Figure 6a for the intermediate CTA batches into R_1 and calculated the transient feed of CTA into R_4. For the change of grade C→A, we pursued a fast but delayed transition. Thus, instead of applying the readjusted plant policy of Figure 6d (which had a tendency to accelerate the change), the following less violent change was introduced at $t = 0$: the CTA load into R_1 was directly changed into the final product value in a single-step change. This direct step change was combined with a transient feed of CTA into R_4.

The optimization results are presented in Table 6 and Figure 7. For both transitions, the off-specs were reduced by ∼60%, with respect to the original plant policy (see Table 6). For the change A→C, the CTA profile exhibits a maximum in the second step, and, thereafter, it is decreasing (Figure 7a). The profile extends for 11 h, and the total added mass of CTA is ∼7 kg. Figure 7c shows a rapid MFI transition, with the switching times of $t_1 = 6.0$ h and $t_2 = 9.5$ h.

For the change C→A, the required CTA transient profile is an ascending "staircase" function. Figure 7f shows a fast but delayed MFI transition, with switching times at $t_1 = 30.2$ h and $t_2 = 34.3$ h. The total added mass of CTA into R_4 was ∼37 kg. The increasing CTA profile into R_4 compensates for the reduced CTA loads into R_1 at $t = 0$. The transient profile reaches its maximum at $t \cong 17$ h, and then it falls to zero at $t \cong 23$ h. This sudden fall of the intermediate CTA feed induces fast transitions into the final values of $\bar{M}_{w,PS}$ and the MFI.

5. Conclusions

A new mathematical model was developed that adequately predicts the steady state (SS) and transient behavior of a continuous high-impact polystyrene (HIPS) process. To the authors' knowledge, this is possibly the first dynamic model that is capable of predicting both the molecular structure and the melt flow index (MFI) of the final product. The MFI is the most important process control variable. It is dependent not only on the free PS molecular weights, but also on the mineral oil content. Fortunately, however, the exponential relationship between the MFI and free PS average molecular weight ($\bar{M}_{w,PS}$) considerably amplifies the relatively small variations of the PS molecular weights in the different grades.

The transitions A⇆B did not require of any optimizations, because of their overlapping MFI specifications. The off-specs accumulation periods of the A⇆C transitions were minimized on the basis of the admissible MFI ranges. In a first level of improvement, the optimizations simply involved readjusting the two intermediate loads of chain transfer agent (CTA) into the dissolver, and through this procedure, the accumulation periods were reduced by 30%, with respect to the original plant policies.

A second level of improvement was also proposed for the A⇆C transitions, which included a transient feed of CTA into the second continuously stirred tank reactor (CSTR). The change A→C involves reducing the average molecular weights, and the control procedure was directed toward a fast and early transition. To this effect, the readjusted policy for the intermediate CTA loads into R_1 was combined with a short (and mainly decreasing) feed profile of CTA into R_4. The change C→A involves increasing the average molecular weights, and the control procedure targeted a fast but delayed transi-

tion. To this effect, a direct step change into the final grade recipe was introduced onto the dissolver at $t = 0$, while an increasing CTA profile was applied onto R_4. According to the model, these procedures reduce the off-spec accumulation periods by ~ 60%, with respect to the original plant policies.

In a future work, a heterogeneous plant model will be developed that is capable of predicting the particle morphology, in addition to the molecular structure and the MFI.

Acknowledgment

We thank Mrs. C. Ocando (University del Zulia, Venezuela) and Mr. J. Perozo (Estizulia C.A., Venezuela) for their help with the industrial experiments. Also, we acknowledge Universidad Nacional del Litoral, ANPCyT, Universidad del Zulia, and our CONICET-FONACIT international agreement for the financial support.

Nomenclature

B* = unreacted butadiene unit
E_{St} = styrene (St) grafting efficiency (%)
f = initiator efficiency (dimensionless)
F_I = molar flow rate of initiator (mol/s)
F_{Oil} = molar flow rate of the mineral oil (mol/s)
F_X = molar flow rate of CTA (mol/s)
G_{GC} = mass flow rate of graft copolymer (g/s)
G_{Gr} = mass flow rate of grafted polystyrene PS (g/s)
G_{PB} = mass flow rate of polybutadiene PB (g/s)
G_{PS} = mass flow rate of free polystyrene PS (g/s)
G_{St} = mass flow rate of styrene St (g/s)
G_{Sv} = mass flow rate of solvent (g/s)
$I^\bullet$ = primary initiator radical
I_F = melt flow index (g/10 min)
I_C = insoluble content (%)
k_d = initiator decomposition rate constant (s^{-1})
k_{fg} = rate constant of chain transfer to the rubber (mol m^{-3} s^{-1})
k_{fm}, k'_{fm} = rate constants of transfer to the monomer (mol m^{-3} s^{-1})
k_{fx}, k'_{fx} = rate constants of transfer to the chain transfer agent (mol m^{-3} s^{-1})
k_{fz}, k'_{fz} = rate constants of transfer to the inhibitor (mol m^{-3} s^{-1})
k_{i0} = rate constant of thermal monomer initiation (mol^2 m^{-6} s^{-1})
k_{i1}, k_{i2} = initiation rate constants (mol m^{-3} s^{-1})
k_p, k_{p0} = propagation rate constants (mol m^{-3} s^{-1})
k_{tc}, k'_{tc} = rate constants of termination by recombination (mol m^{-3} s^{-1})
M_{Bd} = molecular weight of a butadiene repeating unit; M_{Bd} = 54 g/mol
$\overline{M}_n$ = number-average molecular weight (g/mol)
M_{St} = molecular weight of a styrene (St) repeating unit; M_{St} =104 g/mol
M_{Sv} = molecular weight of the solvent; M_{Sv} =106 g/mol
$\overline{M}_w$ = weight-average molecular weight (g/mol)
$P^\bullet$ = nonprimary copolymer radical
$P_B(b)$ = PB molecule with b repetitive units
$P_g(s,b)$ = graft copolymer molecule containing g branches, s repetitive units of styrene St, and b repetitive units of butadiene
P_C = polymer content (%)
$P_S(s)$ = free PS molecule with s repetitive units of styrene
$P_0^\bullet$ = primary copolymer radical
q = outlet volume flow rate (m^3/s)
$\bar{r}_n$ = average number of branches per graft copolymer molecule (dimensionless)
$S^\bullet$ = polystyryl radical
S_C = solid content (%)
t = time (s)
T = temperature (°C)
V = volume (m^3)
x = monomer conversion (%)

Greek Symbols

$\dot{\gamma}$ = shear rate (s^{-1})
$\dot{\epsilon}$ = elongational rate (s^{-1})
η = viscosity (Pa s)
η_0 = zero-shear viscosity (Pa s)
η_e = elongational viscosity (Pa s)
τ_r = relaxation time (s)
ϕ_{Rubb} = volume fraction of the dispersed rubber phase (dimensionless)
ϕ_{Oil} = volume fraction of the mineral oil (dimensionless)
ϕ_P = polymer volume fraction (dimensionless)

Appendix A. Polymerization Model of a Generic Continuously Stirred Tank Reactor

Let r_i (i = 1, 2, ..., 15) be any of the hypothetical continuously stirred tank reactors (CSTRs) in the train, with $r_1 \equiv R_1$; $r_2 \equiv R_2$; $r_3 \equiv R_3$; $r_4 \equiv R_4$; r_5–$r_9 \equiv R_5$; r_{10}–$r_{14} \equiv R_6$; and $r_{15} \equiv R_7$ (see Figure 1). From the kinetic mechanism of Table 4, the following mass balances were derived for the reagents, products, and intermediate free radicals.

Initiator. For the initiator,

$$\frac{d\{[I]_{r_i} V_{r_i}\}}{dt} = q_{r_{i-1}}[I]_{r_{i-1}} - q_{r_i}[I]_{r_i} + F_{I,r_i} - k_{d,r_i}[I]_{r_i} V_{r_i} \quad (A.1)$$

Monomer. If one assumes the "long chain approximation" (by which the monomer is only consumed by the propagation reaction), the monomer mass balance results:

$$\frac{d\{[St]_{r_i} V_{r_i}\}}{dt} = q_{r_{i-1}}[St]_{r_{i-1}} - q_{r_i}[St]_{r_i} - R_{p,r_i} V_{r_i} \quad (A.2)$$

$$R_{p,r_i} = k_{p,r_i}([S^\bullet]_{r_i} + [P^\bullet]_{r_i})[St]_{r_i} \quad (A.3)$$

Chain Transfer Agent. For the chain transfer agent (CTA),

$$\frac{d\{[X]_{r_i} V_{r_i}\}}{dt} = q_{r_{i-1}}[X]_{r_{i-1}} - q_{r_i}[X]_{r_i} + F_{X,r_i} - \{k_{fx,r_i}([S^\bullet]_{r_i} + [P^\bullet]_{r_i}) + k'_{fx,r_i}[P_0^\bullet]_{r_i}\}[X]_{r_i} V_{r_i} \quad (A.4)$$

Inhibitor. For the inhibitor,

$$\frac{d\{[Z]_{r_i} V_{r_i}\}}{dt} = q_{r_{i-1}}[Z]_{r_{i-1}} - q_{r_i}[Z]_{r_i} - \{k_{fz,r_i}([S^\bullet]_{r_i} + [P^\bullet]_{r_i}) + k'_{fz,r_i}[P_0^\bullet]_{r_i}\}[Z]_{r_i} V_{r_i} \quad (A.5)$$

Unreacted Butadiene Units. For the unreacted butadiene units,

$$\frac{\mathrm{d}\{[\mathrm{B}^*]_{\mathrm{r}_i}V_{\mathrm{r}_i}\}}{\mathrm{d}t} = q_{\mathrm{r}_{i-1}}[\mathrm{B}^*]_{\mathrm{r}_{i-1}} - q_{\mathrm{r}_i}[\mathrm{B}^*]_{\mathrm{r}_i} - \{k_{\mathrm{i2},\mathrm{r}_i}[\mathrm{I}^\bullet]_{\mathrm{r}_i} + k_{\mathrm{fg},\mathrm{r}_i}([\mathrm{S}^\bullet]_{\mathrm{r}_i} + [\mathrm{P}^\bullet]_{\mathrm{r}_i})\}\,[\mathrm{B}^*]_{\mathrm{r}_i}V_{\mathrm{r}_i} + \{k'_{\mathrm{fm},\mathrm{r}_i}[\mathrm{St}]_{\mathrm{r}_i} + k'_{\mathrm{fx},\mathrm{r}_i}[\mathrm{X}]_{\mathrm{r}_i} + k'_{\mathrm{fz},\mathrm{r}_i}[\mathrm{Z}]_{\mathrm{r}_i}\}\,[\mathrm{P}_0^\bullet]_{\mathrm{r}_i}V_{\mathrm{r}_i} \quad (A.6)$$

Oil and Solvent. For the oil and solvent,

$$\frac{\{[\mathrm{Oil}]_{\mathrm{r}_i}V_{\mathrm{r}_i}\}}{\mathrm{d}t} = q_{\mathrm{r}_{i-1}}[\mathrm{Oil}]_{\mathrm{r}_{i-1}} - q_{\mathrm{r}_i}[\mathrm{Oil}]_{\mathrm{r}_i} + F_{\mathrm{Oil},\mathrm{r}_i} \quad (A.7)$$

$$\frac{\mathrm{d}\{[\mathrm{Sv}]_{\mathrm{r}_i}V_{\mathrm{r}_i}\}}{\mathrm{d}t} = q_{\mathrm{r}_{i-1}}[\mathrm{Sv}]_{\mathrm{r}_{i-1}} - q_{\mathrm{r}_i}[\mathrm{Sv}]_{\mathrm{r}_i} \quad (A.8)$$

Free Polystyrene (PS). We define the following kinetic parameters:

$$\varphi_{\mathrm{r}_i} = \frac{[\mathrm{S}^\bullet]_{\mathrm{r}_i}}{[\mathrm{S}^\bullet]_{\mathrm{r}_i} + [\mathrm{P}^\bullet]_{\mathrm{r}_i}} \quad (A.9)$$

$$\beta_{\mathrm{r}_i} = \frac{k_{\mathrm{tc},\mathrm{r}_i}R_{\mathrm{p},\mathrm{r}_i}}{(k_{\mathrm{p},\mathrm{r}_i}[\mathrm{St}]_{\mathrm{r}_i})^2} \quad (A.10)$$

$$\tau_{1,\mathrm{r}_i} = \frac{k''_{\mathrm{tc},\mathrm{r}_i}R_{\mathrm{p},\mathrm{r}_i}}{(k_{\mathrm{p},\mathrm{r}_i}[\mathrm{St}]_{\mathrm{r}_i})^2} \quad (A.11)$$

$$\gamma_{\mathrm{r}_i} = \frac{[\mathrm{P}_0^\bullet]_{\mathrm{r}_i}}{[\mathrm{P}^\bullet]_{\mathrm{r}_i} + [\mathrm{S}^\bullet]_{\mathrm{r}_i}} \quad (A.12)$$

$$\tau_{\mathrm{r}_i} = \frac{k_{\mathrm{fm},\mathrm{r}_i}}{k_{\mathrm{p},\mathrm{r}_i}} + \frac{k_{\mathrm{fx},\mathrm{r}_i}[\mathrm{X}]_{\mathrm{r}_i}}{k_{\mathrm{p},\mathrm{r}_i}[\mathrm{St}]_{\mathrm{r}_i}} + \frac{k_{\mathrm{fz},\mathrm{r}_i}[\mathrm{Z}]_{\mathrm{r}_i}}{k_{\mathrm{p},\mathrm{r}_i}[\mathrm{St}]_{\mathrm{r}_i}} + \frac{k_{\mathrm{fg},\mathrm{r}_i}[\mathrm{B}^*]_{\mathrm{r}_i}}{k_{\mathrm{p},\mathrm{r}_i}[\mathrm{St}]_{\mathrm{r}_i}} + \gamma_{\mathrm{r}_i}\tau_{1,\mathrm{r}_i} \quad (A.13)$$

$$\alpha_{\mathrm{r}_i} = \tau_{\mathrm{r}_i} + \beta_{\mathrm{r}_i} \quad (A.14)$$

The mass balance for the free PS then results:

$$\frac{\mathrm{d}\{[\mathrm{P}_\mathrm{S}(s)]_{\mathrm{r}_i}V_{\mathrm{r}_i}\}}{\mathrm{d}t} = q_{\mathrm{r}_{i-1}}[\mathrm{P}_\mathrm{S}(s)]_{\mathrm{r}_{i-1}} - q_{\mathrm{r}_i}[\mathrm{P}_\mathrm{S}(s)]_{\mathrm{r}_i} + \left\{\varphi_{\mathrm{r}_i}(\tau_{\mathrm{r}_i} - \gamma_{\mathrm{r}_i}\tau_{1,\mathrm{r}_i}) + \frac{\varphi_{\mathrm{r}_i}^2\beta_{\mathrm{r}_i}}{2}\alpha_{\mathrm{r}_i}s\right\}R_{\mathrm{p},\mathrm{r}_i}V_{\mathrm{r}_i}\alpha_{\mathrm{r}_i}\mathrm{e}^{-\alpha_{\mathrm{r}_i}s} \quad (A.15)$$

where s ($s = 1, 2, \ldots$) is the number of styrene (St) repetitive units. Equation A.15 calculates the number-chain length distribution (NCLD) of the free PS.

Residual PB. For the residual PB,

$$\frac{\mathrm{d}\{[\mathrm{P}_\mathrm{B}(b)]_{\mathrm{r}_i}V_{\mathrm{r}_i}\}}{\mathrm{d}t} = q_{\mathrm{r}_{i-1}}[\mathrm{P}_\mathrm{B}(b)]_{\mathrm{r}_{i-1}} - q_{\mathrm{r}_i}[\mathrm{P}_\mathrm{B}(b)]_{\mathrm{r}_i} - R_{\mathrm{p},\mathrm{r}_i}V_{\mathrm{r}_i}\left\{(1-\varphi_{\mathrm{r}_i})\left[\tau_{\mathrm{r}_i} + \varphi_{\mathrm{r}_i}\tau_{1,\mathrm{r}_i} + \beta_{\mathrm{r}_i} + \frac{\varphi_{\mathrm{r}_i}\tau_{1,\mathrm{r}_i}\varphi_{\mathrm{r}_i}}{(1-\varphi_{\mathrm{r}_i})}\right] + \frac{R_{\mathrm{p},\mathrm{r}_i}k_{\mathrm{tc},\mathrm{r}_i}\gamma_{\mathrm{r}_i}^2}{(k_{\mathrm{p},\mathrm{r}_i}[\mathrm{St}]_{\mathrm{r}_i})^2}\right\}\frac{b[\mathrm{P}_\mathrm{B}(b)]_{\mathrm{r}_i}}{[\mathrm{B}^*]_{\mathrm{r}_i}} \quad (A.16)$$

where b ($b = 1, 2, \ldots$) is the number of Bd repetitive units. Equation A.16 calculates the NCLD of the residual PB.

Graft Copolymer. For the graft copolymer, let s and b be the number of St and Bd repetitive units, respectively, and let g be the number of PS branches. In the following, s, b, g, and the intermediate variable m can adopt any integer value from 1 to infinity. Following Estenoz et al.,[7] the graft copolymer mass balance results:

$$\frac{\mathrm{d}\{[\mathrm{P}_g(s,b)]_{\mathrm{r}_i}V_{\mathrm{r}_i}\}}{\mathrm{d}t} = q_{\mathrm{r}_i-1}[\mathrm{P}_g(s,b)]_{\mathrm{r}_{i-1}} - q_{\mathrm{r}_i}[\mathrm{P}_g(s,b)]_{\mathrm{r}_i} + G_{1,\mathrm{r}_i} + G_{2,\mathrm{r}_i} + G_{3,\mathrm{r}_i} \quad (A.17)$$

with

$$G_{1,\mathrm{r}_i} = -b[\mathrm{P}_g(s,b)]_{\mathrm{r}_i}\{k_{\mathrm{i2},\mathrm{r}_i}[\mathrm{I}^\bullet]_{\mathrm{r}_i} + k_{\mathrm{fg},\mathrm{r}_i}([\mathrm{S}^\bullet]_{\mathrm{r}_i} + [\mathrm{P}^\bullet]_{\mathrm{r}_i})\}V_{\mathrm{r}_i} \quad (A.18)$$

$$G_{2,\mathrm{r}_i} = \{k_{\mathrm{fm},\mathrm{r}_i}[\mathrm{St}]_{\mathrm{r}_i} + k_{\mathrm{fx},\mathrm{r}_i}[\mathrm{X}]_{\mathrm{r}_i} + k_{\mathrm{fg},\mathrm{r}_i}[\mathrm{B}^*]_{\mathrm{r}_i}\} \times \frac{(1-\varphi_{\mathrm{r}_i})R_{\mathrm{p},\mathrm{r}_i}}{k_{\mathrm{p},\mathrm{r}_i}[\mathrm{St}]_{\mathrm{r}_i}}V_{\mathrm{r}_i}\sum_{m=1}^{s}\frac{\alpha_{\mathrm{r}_i}}{(1+\alpha_{\mathrm{r}_i})^m}\frac{b[\mathrm{P}_{g-1}(s-m,b)]_{\mathrm{r}_i}}{[\mathrm{B}^*]_{\mathrm{r}_i}} + k_{\mathrm{tc},\mathrm{r}_i}\frac{(1-\varphi_{\mathrm{r}_i})\varphi_{\mathrm{r}_i}(R_{\mathrm{p},\mathrm{r}_i})^2}{(k_{\mathrm{p},\mathrm{r}_i}[\mathrm{St}]_{\mathrm{r}_i})^2}V_{\mathrm{r}_i} \times \sum_{m=1}^{s}\frac{(\alpha_{\mathrm{r}_i})^2}{(1+\alpha_{\mathrm{r}_i})^m}\frac{b[\mathrm{P}_{g-1}(s-m,b)]_{\mathrm{r}_i}}{[\mathrm{B}^*]_{\mathrm{r}_i}} + k''_{\mathrm{tc},\mathrm{r}_i}\frac{\varphi_{\mathrm{r}_i}R_{\mathrm{p},\mathrm{r}_i}}{k_{\mathrm{p},\mathrm{r}_i}[\mathrm{St}]_{\mathrm{r}_i}}[\mathrm{P}_0^\bullet]_{\mathrm{r}_i}V_{\mathrm{r}_i}\sum_{m=1}^{s}\frac{\alpha_{\mathrm{r}_i}}{(1+\alpha_{\mathrm{r}_i})^m}\frac{b[\mathrm{P}_{g-1}(s-m,b)]_{\mathrm{r}_i}}{[\mathrm{B}^*]_{\mathrm{r}_i}} \quad (A.19)$$

$$G_{3,\mathrm{r}_i} = \{k'_{\mathrm{fm},\mathrm{r}_i}[\mathrm{St}]_{\mathrm{r}_i} + k'_{\mathrm{fx},\mathrm{r}_i}[\mathrm{X}]_{\mathrm{r}_i}\}\frac{b[\mathrm{P}_g(s,b)]_{\mathrm{r}_i}}{[\mathrm{B}^*]_{\mathrm{r}_i}}[\mathrm{P}_0^\bullet]_{\mathrm{r}_i}V_{\mathrm{r}_i} \quad (A.20)$$

Equations A.17−A.20 calculate the bivariate NCLD of the graft copolymer.

Radical Species. Assuming the pseudo-steady-state approximation, the free-radical mass balances result:

$$\frac{\mathrm{d}\{[\mathrm{I}^\bullet]_{\mathrm{r}_i}V_{\mathrm{r}_i}\}}{\mathrm{d}t} = q_{\mathrm{r}_{i-1}}[\mathrm{I}^\bullet]_{\mathrm{r}_{i-1}} - q_{\mathrm{r}_i}[\mathrm{I}^\bullet]_{\mathrm{r}_i} + 2fk_{\mathrm{d},\mathrm{r}_i}[\mathrm{I}]_{\mathrm{r}_i}V_{\mathrm{r}_i} - (k_{\mathrm{i}1,\mathrm{r}_i}[\mathrm{St}]_{\mathrm{r}_i} + k_{\mathrm{i}2,\mathrm{r}_i}[\mathrm{B}^*]_{\mathrm{r}_i})[\mathrm{I}^\bullet]_{\mathrm{r}_i}V_{\mathrm{r}_i} \approx 0 \quad \text{(A.21)}$$

$$\frac{\mathrm{d}\{[\mathrm{S}^\bullet]_{\mathrm{r}_i}V_{\mathrm{r}_i}\}}{\mathrm{d}t} = q_{\mathrm{r}_{i-1}}[\mathrm{S}^\bullet]_{\mathrm{r}_{i-1}} - q_{\mathrm{r}_i}[\mathrm{S}^\bullet]_{\mathrm{r}_i} + k_{\mathrm{i}1,\mathrm{r}_i}[\mathrm{St}]_{\mathrm{r}_i}[\mathrm{I}^\bullet]_{\mathrm{r}_i}V_{\mathrm{r}_i} + 2k_{\mathrm{i}0,\mathrm{r}_i}[\mathrm{St}]_{\mathrm{r}_i}{}^3V_{\mathrm{r}_i} + (k'_{\mathrm{fm},\mathrm{r}_i}[\mathrm{St}]_{\mathrm{r}_i} + k'_{\mathrm{fx},\mathrm{r}_i}[\mathrm{X}]_{\mathrm{r}_i})[\mathrm{P}_0^\bullet]_{\mathrm{r}_i}V_{\mathrm{r}_i} + (k_{\mathrm{fm},\mathrm{r}_i}[\mathrm{St}]_{\mathrm{r}_i} + k_{\mathrm{fx},\mathrm{r}_i}[\mathrm{X}]_{\mathrm{r}_i})[\mathrm{P}^\bullet]_{\mathrm{r}_i}V_{\mathrm{r}_i} - \{k_{\mathrm{fg},\mathrm{r}_i}[\mathrm{B}^*]_{\mathrm{r}_i} + k_{\mathrm{fz},\mathrm{r}_i}[\mathrm{Z}]_{\mathrm{r}_i} + k''_{\mathrm{tc},\mathrm{r}_i}[\mathrm{P}_0^\bullet]_{\mathrm{r}_i} + k_{\mathrm{tc},\mathrm{r}_i}([\mathrm{P}^\bullet]_{\mathrm{r}_i} + [\mathrm{S}^\bullet]_{\mathrm{r}_i})\}\,[\mathrm{S}^\bullet]_{\mathrm{r}_i}V_{\mathrm{r}_i} \approx 0 \quad \text{(A.22)}$$

$$\frac{\mathrm{d}\{[\mathrm{P}_0^\bullet]_{\mathrm{r}_i}V_{\mathrm{r}_i}\}}{\mathrm{d}t} = q_{\mathrm{r}_{i-1}}[\mathrm{P}_0^\bullet]_{\mathrm{r}_{i-1}} - q_{\mathrm{r}_i}[\mathrm{P}_0^\bullet]_{\mathrm{r}_i} + \{k_{\mathrm{i}2,\mathrm{r}_i}[\mathrm{I}^\bullet]_{\mathrm{r}_i} + k_{\mathrm{fg},\mathrm{r}_i}([\mathrm{S}^\bullet]_{\mathrm{r}_i} + [\mathrm{P}^\bullet]_{\mathrm{r}_i})\}\,[\mathrm{B}^*]_{\mathrm{r}_i}V_{\mathrm{r}_i} - \{(k_{\mathrm{p}0,\mathrm{r}_i} + k'_{\mathrm{fm},\mathrm{r}_i})[\mathrm{St}]_{\mathrm{r}_i} + k'_{\mathrm{fx},\mathrm{r}_i}[\mathrm{X}]_{\mathrm{r}_i} + k'_{\mathrm{fz},\mathrm{r}_i}[\mathrm{Z}]_{\mathrm{r}_i} + k''_{\mathrm{tc},\mathrm{r}_i}([\mathrm{P}^\bullet]_{\mathrm{r}_i} + [\mathrm{S}^\bullet]_{\mathrm{r}_i})\}[\mathrm{P}_0^\bullet]_{\mathrm{r}_i}V_{\mathrm{r}_i} \approx 0 \quad \text{(A.23)}$$

$$\frac{\mathrm{d}\{[\mathrm{P}^\bullet]_{\mathrm{r}_i}V_{\mathrm{r}_i}\}}{\mathrm{d}t} = q_{\mathrm{r}_{i-1}}[\mathrm{P}^\bullet]_{\mathrm{r}_{i-1}} - q_{\mathrm{r}_i}[\mathrm{P}^\bullet]_{\mathrm{r}_i} + k_{\mathrm{p}0,\mathrm{r}_i}[\mathrm{St}]_{\mathrm{r}_i}[\mathrm{P}_0^\bullet]_{\mathrm{r}_i}V_{\mathrm{r}_i} - \{k_{\mathrm{fm},\mathrm{r}_i}[\mathrm{St}]_{\mathrm{r}_i} + k_{\mathrm{fx},\mathrm{r}_i}[\mathrm{X}]_{\mathrm{r}_i} + k_{\mathrm{fz},\mathrm{r}_i}[\mathrm{Z}]_{\mathrm{r}_i} + k_{\mathrm{fg},\mathrm{r}_i}[\mathrm{B}^*]_{\mathrm{r}_i} + k''_{\mathrm{tc},\mathrm{r}_i}[\mathrm{P}_0^\bullet]_{\mathrm{r}_i} + k_{\mathrm{tc},\mathrm{r}_i}([\mathrm{P}^\bullet]_{\mathrm{r}_i} + [\mathrm{S}^\bullet]_{\mathrm{r}_i})\}\,[\mathrm{P}^\bullet]_{\mathrm{r}_i}V_{\mathrm{r}_i} \approx 0 \quad \text{(A.24)}$$

Solid Content. For the solid content,

$$S_{\mathrm{C},\mathrm{r}_i} = \frac{G_{\mathrm{PS},\mathrm{r}_i} + G_{\mathrm{PB},\mathrm{r}_i} + G_{\mathrm{GC},\mathrm{r}_i} + G_{\mathrm{Oil},\mathrm{r}_i}}{G_{\mathrm{PS},\mathrm{r}_i} + G_{\mathrm{PB},\mathrm{r}_i} + G_{\mathrm{GC},\mathrm{r}_i} + G_{\mathrm{Oil},\mathrm{r}_i} + G_{\mathrm{St},\mathrm{r}_i} + G_{\mathrm{Sv},\mathrm{r}_i}} \quad \text{(A.25)}$$

where the outlet mass flow rates of reagents and products from reactor r_i are given as follows:

$$G_{\mathrm{PS},\mathrm{r}_i} = q_{\mathrm{r}_i}\mathrm{M}_{\mathrm{St}}\sum_{s=2}^{\infty}[\mathrm{P}_{\mathrm{S}}(s)]_{\mathrm{r}_i}s \quad \text{(A.26)}$$

$$G_{\mathrm{PB},\mathrm{r}_i} = q_{\mathrm{r}_i}\mathrm{M}_{\mathrm{Bd}}\sum_{b=1}^{\infty}[\mathrm{P}_{\mathrm{B}}(b)]_{\mathrm{r}_i}b \quad \text{(A.27)}$$

$$G_{\mathrm{GC},\mathrm{r}_i} = q_{\mathrm{r}_i}\sum_{g=1}^{\infty}\sum_{b=1}^{\infty}\sum_{s=1}^{\infty}[\mathrm{P}_g(s,b)]_{\mathrm{r}_i}(s\mathrm{M}_{\mathrm{St}} + b\mathrm{M}_{\mathrm{Bd}}) \quad \text{(A.28)}$$

$$G_{\mathrm{St},\mathrm{r}_i} = q_{\mathrm{r}_i}\mathrm{M}_{\mathrm{St}}[\mathrm{St}]_{\mathrm{r}_i} \quad \text{(A.29)}$$

$$G_{\mathrm{Sv},\mathrm{r}_i} = q_{\mathrm{r}_i}\mathrm{M}_{\mathrm{Sv}}[\mathrm{Sv}]_{\mathrm{r}_i} \quad \text{(A.30)}$$

$$G_{\mathrm{Oil},\mathrm{r}_i} = q_{\mathrm{r}_i}\overline{\mathrm{M}}_{\mathrm{Oil}}[\mathrm{Oil}]_{\mathrm{r}_i} \quad \text{(A.31)}$$

Polymer Content. For the polymer content,

$$P_{\mathrm{C},\mathrm{r}_i} = \frac{G_{\mathrm{PS},\mathrm{r}_i} + G_{\mathrm{PB},\mathrm{r}_i} + G_{\mathrm{GC},\mathrm{r}_i}}{G_{\mathrm{PS},\mathrm{r}_i} + G_{\mathrm{PB},\mathrm{r}_i} + G_{\mathrm{GC},\mathrm{r}_i} + G_{\mathrm{Oil},\mathrm{r}_i} + G_{\mathrm{St},\mathrm{r}_i} + G_{\mathrm{Sv},\mathrm{r}_i}} \quad \text{(A.32)}$$

Monomer Conversion. We adopt the following dynamic definition for the monomer conversion in reactor r_i:

$$x_{\mathrm{r}_i} = \frac{G_{\mathrm{Gr},\mathrm{r}_i} + G_{\mathrm{PS},\mathrm{r}_i}}{G_{\mathrm{Gr},\mathrm{r}_i} + G_{\mathrm{PS},\mathrm{r}_i} + G_{\mathrm{St},\mathrm{r}_i}} \quad \text{(A.33)}$$

where $G_{\mathrm{Gr},\mathrm{r}_i}$ is the mass flow rate of grafted styrene St, which, in turn, is obtained from

$$G_{\mathrm{Gr},\mathrm{r}_i} = q_{\mathrm{r}_i}\sum_{g=1}^{\infty}\sum_{b=1}^{\infty}\sum_{s=1}^{\infty}[\mathrm{P}_g(s,b)]_{\mathrm{r}_i}(s\mathrm{M}_{\mathrm{St}}) \quad \text{(A.34)}$$

Insoluble Content. For the insoluble content,

$$I_{\mathrm{C},\mathrm{r}_i} = \frac{G_{\mathrm{GC},\mathrm{r}_i} + G_{\mathrm{PB},\mathrm{r}_i}}{G_{\mathrm{PS},\mathrm{r}_i} + G_{\mathrm{GC},\mathrm{r}_i} + G_{\mathrm{PB},\mathrm{r}_i}} \quad \text{(A.35)}$$

Grafting Efficiency. For the grafting efficiency,

$$E_{\mathrm{St},\mathrm{r}_i} = \frac{G_{\mathrm{Gr},\mathrm{r}_i}}{G_{\mathrm{PS},\mathrm{r}_i} + G_{\mathrm{Gr},\mathrm{r}_i}} \quad \text{(A.36)}$$

Average Molecular Weights. The average molecular weights of the free PS, residual PB, and graft copolymer are calculated from their NCLDs as follows:

$$\overline{M}_{\mathrm{n,PS}} = \mathrm{M}_{\mathrm{St}}\frac{\sum_s[\mathrm{P}_{\mathrm{S}}(s)]_{\mathrm{r}_i}s}{\sum_s[\mathrm{P}_{\mathrm{S}}(s)]_{\mathrm{r}_i}} \quad \text{(A.37)}$$

$$\overline{M}_{\mathrm{w,PS}} = \mathrm{M}_{\mathrm{St}}\frac{\sum_s[\mathrm{P}_{\mathrm{S}}(s)]_{\mathrm{r}_i}s^2}{\sum_s[\mathrm{P}_{\mathrm{S}}(s)]_{\mathrm{r}_i}s} \quad \text{(A.38)}$$

$$\overline{M}_{\mathrm{n,PB}} = \mathrm{M}_{\mathrm{Bd}}\frac{\sum_b[\mathrm{P}_{\mathrm{B}}(b)]_{\mathrm{r}_i}b}{\sum_b[\mathrm{P}_{\mathrm{B}}(b)]_{\mathrm{r}_i}} \quad \text{(A.39)}$$

$$\overline{M}_{\mathrm{w,PB}} = \mathrm{M}_{\mathrm{Bd}}\frac{\sum_b[\mathrm{P}_{\mathrm{B}}(b)]_{\mathrm{r}_i}b^2}{\sum_b[\mathrm{P}_{\mathrm{B}}(b)]_{\mathrm{r}_i}b} \quad \text{(A.40)}$$

$$\overline{M}_{\mathrm{n,C}} = \frac{\sum_s\sum_b\sum_g[\mathrm{P}_g(s,b)]_{\mathrm{r}_i}(s\mathrm{M}_{\mathrm{St}} + b\mathrm{M}_{\mathrm{Bd}})}{\sum_s\sum_b\sum_g[\mathrm{P}_g(s,b)]_{\mathrm{r}_i}} \quad \text{(A.41)}$$

$$\overline{M}_{\mathrm{w,C}} = \frac{\sum_s\sum_b\sum_g[\mathrm{P}_g(s,b)]_{\mathrm{r}_i}(s\mathrm{M}_{\mathrm{St}} + b\mathrm{M}_{\mathrm{Bd}})^2}{\sum_s\sum_b\sum_g[\mathrm{P}_g(s,b)]_{\mathrm{r}_i}(s\mathrm{M}_{\mathrm{St}} + b\mathrm{M}_{\mathrm{Bd}})} \quad \text{(A.42)}$$

Number-Average Number of Styrene Branches per Copolymer Molecule. For the number-average

number of styrene (St) branches per copolymer molecule:

$$\bar{r}_n = \frac{\sum_s \sum_b \sum_g [\mathrm{P}_g(s,b)]_{\mathrm{r}_i} g}{\sum_s \sum_b \sum_g [\mathrm{P}_g(s,b)]_{\mathrm{r}_i}} \tag{A.43}$$

Volume Fraction of Polymer in the Reaction Mixture. For the volume fraction of polymer in the reaction mixture,

$$\phi_{\mathrm{P},\mathrm{r}_i} = \frac{\sum_{j=\mathrm{GC,PB,PS}} \mathrm{G}_{j,\mathrm{r}_i}/\rho_j}{\sum_{j=\mathrm{GC,PB,PS,St,Sv,Oil}} \mathrm{G}_{j,\mathrm{r}_i}/\rho_j} \tag{A.44}$$

Final Volume Fractions of Mineral Oil and Total Rubber in the Final High-Impact Polystyrene. For the final volume fractions of mineral oil and total rubber in the final HIPS,

$$\phi_{\mathrm{Oil}} = \frac{\mathrm{G}_{\mathrm{Oil},\mathrm{r}_{15}}/\rho_{\mathrm{Oil}}}{\sum_{i=\mathrm{GC,PB,PS,Oil}} \mathrm{G}_{i,\mathrm{r}_{15}}/\rho_i} \tag{A.45}$$

$$\phi_{\mathrm{Rubb}} = \frac{\sum_{i=\mathrm{GC,PB}} \mathrm{G}_{i,\mathrm{r}_{15}}/\rho_i}{\sum_{i=\mathrm{GC,PB,PS}} \mathrm{G}_{i,\mathrm{r}_{15}}/\rho_i} \tag{A.46}$$

Equation A.46 estimates the volume fraction of the PB + graft copolymer mixture in the (oil-free) polymer.

Density of the Final High-Impact Polystyrene. For the density of the final HIPS,

$$\rho = \sum_{i=\mathrm{GC,Oil,PS,PB}} w_i \rho_i \tag{A.47}$$

where the mass fractions of the four HIPS components are given as follows:

$$w_i = \frac{G_{i,\mathrm{r}_{15}}}{\sum_{j=\mathrm{GC,Oil,PS,PB}} G_{j,\mathrm{r}_{15}}} \qquad (\text{for } i = \mathrm{GC, Oil, PS, PB}) \tag{A.48}$$

Appendix B. Melt Flow Index Model

The melt flow index (MFI, denoted as I_F) is the mass flow rate (in units of g/10 min) of a HIPS melt that flows through a plastometer capillary when forced by a piston that is loaded with a constant weight. The polymer accumulates in a barrel, prior to entering into the capillary. Between the barrel and the capillary, there is an abrupt contraction or "entrance" zone.

First, consider estimating the shear viscosity function $\eta(\dot{\gamma})$, where η the apparent shear viscosity and $\dot{\gamma}$ is the apparent shear rate. The following three-parameter expression is proposed:[22,23]

$$\eta(\dot{\gamma}) = \frac{\eta_0}{[1 + (\tau_\mathrm{r}\dot{\gamma})^2]^{n'/2}} \tag{B.1}$$

where η_0 is the zero-shear viscosity, τ_r the relaxation time, and n' the slope of the final asymptote of log η vs log $\dot{\gamma}$. The value of n' was taken from the literature[17] (see Table 5). For τ_r, we used[22,23]

$$\tau_\mathrm{r} = \frac{6\eta_0 \overline{M}_{\mathrm{w,PS}}}{\pi^2 \rho \mathrm{RT}} \tag{B.2}$$

For η_0, we adopted a logarithmic mixing rule that takes into account the mineral oil:[24]

$$\ln \eta_0 = (1 - \phi_{\mathrm{Oil}}) \ln \eta_{0,\mathrm{P}} + \phi_{\mathrm{Oil}} \ln \eta_{0,\mathrm{Oil}} \tag{B.3}$$

where $\eta_{0,\mathrm{P}}$ is the zero-shear viscosity of the (oil-free) polymer, $\eta_{0,\mathrm{Oil}}$ the measured zero-shear viscosity of the mineral oil (see Table 2), and ϕ_{Oil} the mineral oil volume fraction (obtained using eq A.45). The polymer zero-shear viscosity is calculated through the Mooney expression:[16]

$$\eta_{0,\mathrm{P}} = \eta_{0,\mathrm{PS}}\, \mathrm{e}^{A\phi_\mathrm{D}/(1-B\phi_\mathrm{D})} \tag{B.4}$$

where $\eta_{0,\mathrm{PS}}$ is the zero-shear viscosity of the free PS; A and B are constants, and ϕ_D is the volume fraction of the dispersed phase in the (oil-free) polymer. The constant B was taken from the literature,[16] and the constant A was adjusted to the MFI measurements (see Table 5). To estimate ϕ_D, we assumed $\phi_\mathrm{D} = \phi_{\mathrm{Rubb}}$ (eq A.46). This produces a ϕ_D by defect, because ϕ_{Rubb} does not include the occluded PS that is contained in the rubber particles. Finally, $\eta_{0,\mathrm{PS}}$ is estimated from[16]

$$\ln \eta_{0,\mathrm{PS}} = -20.95 + 3.4 \ln\left(\frac{\bar{M}_{\mathrm{w,PS}}}{33\,000}\right) + \frac{11\,000}{T} \tag{B.5}$$

where $\bar{M}_{\mathrm{w,PS}}$ is calculated using eq A.38.

From the knowledge of $\eta(\dot{\gamma})$, consider the model by Seavey et al.[15] The model assumptions are as follows: (a) steady-state flow; (b) zero velocity at the capillary wall; and (c) the elongational viscosity is 3 times the shear viscosity (the Trouton's ratio). Assumption (b) is generally valid for homogeneous systems,[22] but, here, it is applied to a heterogeneous material.

The following nomenclature is used: R_b and L_b are the respective radius and length of the barrel; R_c and L_c are the respective radius and length of the capillary; R_p is the radius of the piston; ΔP_b, ΔP_e, ΔP_c are the respective pressure decreases in the barrel, entrance zone, and capillary, respectively; m is the piston weight; g is the gravity constant; $(\eta_{R_\mathrm{b}}, \dot{\gamma}_{R_\mathrm{b}})$ is the pair of shear viscosity−shear rate at the barrel wall; $(\eta_{R_\mathrm{c}}, \dot{\gamma}_{R_\mathrm{c}})$ is the pair of shear viscosity−shear rate at the capillary wall; $(\eta_{\mathrm{a,c}}, \dot{\gamma}_\mathrm{a})$ is the pair of apparent shear viscosity−apparent shear rate in the capillary; and $(\eta_{\mathrm{e,c}}, \dot{\epsilon}_\mathrm{a})$ is the pair of apparent elongational viscosity−apparent elongational rate in the capillary.

The MFI is given by

$$I_\mathrm{F} = \rho Q \tag{B.6}$$

where Q is the volume flow rate and ρ is the density of the melt (obtained from eq A.47). In turn, Q is related to the viscosity function in the barrel and capillary, through the following balances:[15,25]

$$Q = \frac{\pi R_c^3 \dot{\gamma}_{R_c}}{3} - \frac{\pi}{3}\left(\frac{2L_c}{\Delta P_c}\right)^3 \int_0^{\dot{\gamma}_{R_c}} [\eta(\dot{\gamma})\dot{\gamma}]^3 d\dot{\gamma} \quad \text{(B.7)}$$

$$Q = \frac{\pi R_b^3 \dot{\gamma}_{R_b}}{3} - \frac{\pi}{3}\left(\frac{2L_b}{\Delta P_b}\right)^3 \int_0^{\dot{\gamma}_{R_b}} [\eta(\dot{\gamma})\dot{\gamma}]^3 d\dot{\gamma} \quad \text{(B.8)}$$

$$\dot{\gamma}_{R_c}\eta_{R_c} = \frac{\Delta P_c R_c}{2L_c} \quad \text{(B.9)}$$

$$\dot{\gamma}_{R_b}\eta_{R_b} = \frac{\Delta P_b R_b}{2L_b} \quad \text{(B.10)}$$

where η_{R_c} and η_{R_b} are respectively calculated from $\dot{\gamma}_{R_c}$ and $\dot{\gamma}_{R_b}$, through $\eta(\dot{\gamma})$. The total pressure decrease is given as

$$\Delta P_b + \Delta P_e + \Delta P_c = \frac{mg}{\pi R_p^2} \quad \text{(B.11)}$$

In turn, ΔP_e is estimated as in the work of Rohlfing and Janzen:[25]

$$\Delta P_e = \frac{4\sqrt{2}\dot{\gamma}_a}{3(n'+1)}\left(\frac{4n'}{3n'+1}\right)^{(1+n'/2)} \sqrt{\eta_{a,c}\eta_{e,c}} \quad \text{(B.12)}$$

where n' was defined in eq B.1. Rohlfing and Janzen[25] also proposed the following expressions for $\dot{\gamma}_a$ and $\dot{\epsilon}_a$:

$$\dot{\gamma}_a = \left(\frac{4}{3 + 1/n'}\right)\gamma_{R_c} \quad \text{(B.13)}$$

$$\dot{\epsilon}_a = \frac{4\eta_{a,c}\dot{\gamma}_a}{3(n'+1)\Delta P_e}\left(\frac{4n'}{3n'+1}\right)^{n'+1} \quad \text{(B.14)}$$

Finally, the Trouton ratio is given as

$$\eta_e(\dot{\epsilon}) = 3\eta(\dot{\gamma}) \quad \text{(B.15)}$$

The pair ($\eta_{a,c}$, $\dot{\gamma}_a$) is interrelated through eq B.1. Similarly, the pair ($\eta_{e,c}$,$\dot{\epsilon}_a$) is interrelated through eqs B.1 and B.15, with $\dot{\gamma} = \dot{\epsilon}_a$.[15]

In eqs B.1−B.15, the known inputs are as follows: $R_b = 4.78$ mm, $R_c = 1.05$ mm, $R_p = 4.74$ mm, $L_b = 46$ mm, $L_c = 8$ mm, $m = 5$ kg, and $g = 9.8$ m/s^2. The unknowns are denoted as follows: I_F, Q, ΔP_b, ΔP_e, ΔP_c, $\dot{\gamma}_{R_b}$, $\dot{\gamma}_{R_c}$, $\dot{\gamma}_a$, $\dot{\epsilon}_a$, η_{R_b}, η_{R_c}, $\eta_{a,c}$, and $\eta_{e,c}$.

Literature Cited

(1) Keskkula, H.; Turley, S. G.; Boyer, R. F. The Significance of the Rubber Damping Peak in Rubber-Modified Polymers. *J. Appl. Polym. Sci*. **1971**, *15*, 351.

(2) Turley, S. G.; Keskkula, H. Effect of Rubber-Phase Volume Fraction in Impact Polystyrene on Mechanical Behaviour. *Polymer* **1980**, *21*, 466.

(3) Piorkowska, E.; Argon, A. S.; Cohen, R. E. Size Effect of Compliant Rubbery Particles on Craze Plasticity in Polystyrene. *Macromolecules* **1990**, *23*, 3838.

(4) Okamoto, Y.; Miyagi, H.; Kakugo, M.; Takahashi, K. Impact Improvement Mechanism of HIPS with Bimodal Distribution of Rubber Particle Size. *Macromolecules* **1991**, *24*, 5639.

(5) Dağli, G.; Argon, A. S.; Cohen, R. E. Particle-Size Effect in Craze Plasticity of High-Impact Polystyrene. *Polymer* **1995**, *36*, 2173.

(6) Katime, I.; Quintana, J. R.; Price, C. Influence of Microstructural Morphology on the Mechanical Properties of High-Impact Polystyrene. *Mater. Lett.* **1995**, *22*, 297.

(7) Estenoz, D. A.; Meira, G. R.; Gómez, N.; Oliva, H. M. Mathematical Model of a Continuous Industrial High-Impact Polystyrene Process. *AIChE J.* **1998**, *44*, 427.

(8) Eliçabe, G. E.; Meira, G. R. Estimation and Control in Polymerization Reactors. A Review. *Polym. Eng. Sci.* **1988**, *28*, 121.

(9) Estenoz, D. A.; Valdez, E.; Oliva, H. M.; Meira, G. R. Bulk Polymerization of Styrene in the Presence of Polybutadiene: Calculation of Molecular Macrostructure. *J. Appl. Polym. Sci.* **1996**, *59*, 861.

(10) Estenoz, D. A.; González, I. M.; Oliva, H. M.; Meira, G. R. Polymerization of Styrene in the Presence of Polybutadiene: Determination of the Molecular Structure. *J. Appl. Polym. Sci.* **1999**, *74*, 1950.

(11) Ludwico, W. A.; Rosen, S. L. The Kinetics of Two-Phase Polymerization. I. Monomer and Initiator Distribution. *J. Appl. Polym. Sci.* **1975**, *19*, 757.

(12) Na, S. S.; Rhee, H. K. An Experimental Study for Property Control in a Continuous Styrene Polymerization Reactor Using a Polynomial ARMA Model. *Chem. Eng. Sci.* **2002**, *57*, 1165.

(13) Flores-Tlacuahuac, A.; Biegler, L. T.; Saldívar-Guerra, E. Dynamic Optimization of HIPS Open-Loop Unstable Polymerization Reactors. *Ind. Eng. Chem. Res.* **2005**, *44,* 2659.

(14) Flores-Tlacuahuac, A.; Zavala-Tejeda, V.; Saldívar-Guerra, E. Complex Nonlinear Behavior in the Full-Scale High-Impact Polystyrene Process. *Ind. Eng. Chem. Res.* **2005**, *44*, 2802.

(15) Seavey, K. C.; Liu, Y. A.; Khare, N. P.; Bremner, T.; Chen, C. C. Quantifying Relationships among the Molecular Weight Distribution, Non-Newtonian Shear Viscosity, and Melt Index for Linear Polymers. *Ind. Eng. Chem. Res.* **2003**, *42*, 5354.

(16) Kruse, R. L.; Southern, J. H. Viscosities and Normal Stress Coefficients of High-Impact Polystyrene Fluids. *J. Rheol.* **1980**, *24*, 455.

(17) Liang, J. Z.; Ness, J. N. Effect of Die Angle on Flow Behaviour for High Impact Polystyrene Melt. *Polym. Test.* **1997**, *16*, 403.

(18) Reid, R. C.; Prausnitz, J. M.; Sherwood, T. K. Viscosity. *The Properties of Gases and Liquids*, 3rd Edition; McGraw−Hill: New York, 1977.

(19) Brandrup, J.; Immergut, E. H. Physical Constant of Some Important Polymers. *Polymer Handbook*, 2nd Edition; Wiley: New York, 1975.

(20) Danner R. P.; High, M. S. Recommended Procedures. *Handbook of Polymer Solution Thermodynamics*; American Institute of Chemical Engineers (AIChE): New York, 1993.

(21) Nelder, J. A.; Mead, R. A Simplex Method for Function Minimization. *Comput. J.* **1965**, *7*, 308.

(22) Carreau, P. J.; De Kee, D. C.; Chhabra, R. P. Material Functions and Generalized Newtonian Fluid. *Rheology of Polymeric Systems. Principles and Applications*; Hanser/Gardner: New York, 1997.

(23) Elbirli, B.; Shaw, M. T. Time Constant from Shear Viscosity Data. *J. Rheol.* **1978**, *22*, 561.

(24) Bremner, T.; Rudin, A.; Cook, D. G. Melt Flow Index Values and Molecular Weight Distributions of Commercial Thermoplastics. *J. Appl. Polym. Sci.* **1990**, *41*, 1617.

(25) Rohlfing, D. C.; Janzen, J. What is Happening in the Melt-Flow Plastometer: The Role of Elongational Viscosity. *Ann. Technol. Conf. Soc. Plast. Eng*. **1997**, 1010.

Received for review June 7, 2005
Revised manuscript received August 13, 2005
Accepted August 19, 2005

IE050657Z